Chemical Physics 543 (2021) 111097

Contents lists available at ScienceDirect

Chemical Physics

journal homepage: www.elsevier.com/locate/chemphys

A modified dynamic lattice searching method for structural optimization of metal oxide clusters

Di Wei [a], Wen Ma [a], Xia Wu [b,*], Longjiu Cheng [a,*]

[a] Department of Chemistry, Anhui Province Key Laboratory of Chemistry for Inorganic/Organic Hybrid Functionalized Materials, Auhui University, Hefei, Anhui 230601, PR China

[b] School of Chemistry and Chemical Engineering, Anqing Normal University, Anqing, Anhui 246011, PR China

ARTICLE INFO

Keywords:
Metal oxide clusters
Stable structures
Structural optimization
Rigid-ion model
Relative stability

ABSTRACT

The stable structures of metal oxide clusters were obtained using a modified dynamic lattice searching (DLS) method with a classic rigid-ion model. Due to the important effect of the electrostatic charge force on the structure of metal oxide clusters, the clusters with various formal charges of metal (q), i.e., $(M^{+2}O)_n$, $(M_3^{+2.67}O_4)_n$, $(M_2^{+3}O_3)_n$, $(M^{+4}O_2)_n$, $(M_2^{+5}O_5)_n$ and $(M^{+6}O_3)_n$, were investigated. Results showed that $(MO)_n$ clusters preferred to form highly coordinated structures, and $(M_3O_4)_n$ clusters generally adopt cage-based structures. When q value was larger, the lowest energy clusters tended to form some compact structures with one or two dangling M═O bonds, even more. Finally, the relationship between the number of M═O bond and the q values were discussed.

1. Introduction

Metal oxide clusters have attracted wide interest owing to their interesting properties, such as catalytic, electronic, and optical properties [1]. For instance, ZnO, a semiconductor with a band gap of 3.37 eV at 300 K and a high exciton binding energy of 60 meV, has been recognized as a valuable optical material in the ultra violet and light-emitting devices [2]. TiO_2 also has a large band gap (3–3.2 eV), and it has been widely applied in photoelectrolysis of water as photocatalytic materials [3]. Furthermore, metal oxide clusters have been successfully fabricated and used as nanoscale sensors and transducers [4–6]. Though they have been developed into various applications, the atomic structures of clusters formed by metal oxides are still not fully studied. It is well known that the evolution from clusters to bulk solids involves structural reconstruction and variations in properties. In order to clarify the properties of metal oxide clusters, it is necessary to have a thorough study of their configurations and growth rules.

Studies relative to metal oxide clusters were developed both experimentally and theoretically. The structures of $(ZnO)_{2\text{-}18}$ clusters were studied based on gradient-corrected density-functional theory (DFT), and it was found that the lowest-energy structures evolved from ring toward cage or tube [7]. The structure of $(ZnO)_{12}$ was a truncated octahedron composed of six $(ZnO)_2$ and eight $(ZnO)_3$ rings with T_h symmetry. Based on this structure, Zhang et al. introduced a beaded ZnO nanocluster as a novel stand-alone system, and found that it had higher chemical reactivity during the growth process [8]. Moreover, for $(MgO)_{3k}$ clusters, the hexagonal tubes were the most stable structures at $k = 1$–5, which were proved by theoretical prediction and spectral experiments [9,10]. The $(V_2O_5)_n$ clusters were predicted to have polyhedral cage structures, which can be used as an ideal molecular model for oxide surfaces and catalysts [11,12]. In addition, TiO_2 [13–16], WO_3 [17,18], Ge_2O_3 [19], Fe_2O_3 [20]and other metal oxide clusters [21–31] were also investigated. However, it was found that the structures of clusters with higher metal charge tended to carry the terminal O-atoms, but the clusters with lower metal charge were not. Whether this phenomenon was only related to the charge of metal attracted our attention. Previously, Johnston et al. studied the structures of MgO clusters and found that their structural types depended on ionic charges of both metal and oxygen: a cubic motif for lower formal charges and hollow cages for higher formal charges [32]. This result showed that charge played an important role in the growth of structures of metal oxide clusters.

On the other hand, it was also a challenge to determine the ground states of metal oxide clusters. Many global optimization algorithms have been extensively developed to understand the lowest-energy structures of metal oxide clusters [22,33–36]. The basin hopping (BH) [37] method and its variants were adopted to study $Ce_{19}O_{32}$ [38], $[Cr_6O_{19}]^{2-}$ [39] and other clusters [40–43]. Based on genetic algorithm (GA), a variety of

* Corresponding authors.
E-mail addresses: xiawu@aqnu.edu.cn (X. Wu), clj@ustc.edu (L. Cheng).

https://doi.org/10.1016/j.chemphys.2021.111097
Received 28 August 2020; Received in revised form 16 December 2020; Accepted 3 January 2021
Available online 7 January 2021

codes were written for the study of ZnO [7], MgO [10,32], BeO [22], TiO_2 [15], and Al_2O_3 clusters [44]. Moreover, the particle swarm optimization algorithms (PSO) and artificial bee colony algorithms (ABCluster) were also developed for the optimization of metal oxide clusters, e.g, MgO [45], TiO_2 [16], and FeO [46]. The dynamic lattice searching (DLS) method showed good efficiency in optimizing monoatomic clusters, such as Lennard-Jones (LJ) clusters [47–49], Morse clusters [50], Al clusters [51–53] and $(C_{60})_n$ clusters [54], and binary clusters, e.g., binary LJ clusters [55] and Au-Pd clusters [56]. Moreover, DLS method was also adopted into the fuzzy global optimization algorithm [57] to improve efficiency. The idea of DLS algorithm was to construct vacant dynamic lattice (DL) around the structures, and the lowest energy structure was found by lattice searching operation. However, for metal (M) oxide system, the M-type atoms are generally near the O atoms due to the influence of Coulomb force, and the original DL in DLS algorithm needs to be modified.

In the present work, the DLS method was modified to study the stable structures of metal oxide clusters. The classical interatomic potentials [23] was applied to geometrical optimization of metal oxide clusters with different metal charges, and the stable structures of $(M^{+2}O)_n$ (n = 1–60), $(M_3^{+2.67}O_4)_n$ (n = 1–15), $(M_2^{+3}O_3)_n$ (n = 1–20), $(M^{+4}O_2)_n$ (n = 1–40), $(M_2^{+5}O_5)_n$ (n = 1–15) and $(M^{+6}O_3)_n$ (n = 1–30) clusters were obtained. The growth rules of metal oxide clusters with different metal charges were studies, and the differences of between structures and relative stability were discussed.

2. Methods

2.1. Potential energy function

The rigid-ion model was applied to describe the interaction of metal oxide clusters [32]. The total energy E and the pair potential of two atoms $V(r_{ij})$ was calculated by

$$E = \sum_i^{N-1}\sum_{j=i+1}^{N} V(r_{ij}) \tag{1}$$

$$V(r_{ij}) = \frac{q_i q_j}{r_{ij}} + \frac{A}{r_{ij}^{12}} - \frac{C}{r_{ij}^{6}} + B\exp\left(\frac{-r_{ij}}{\rho}\right) \tag{2}$$

where r_{ij} was the distance between two atoms, and N was the number of atoms in clusters. In the equation, the first term was simply the coulomb contrubution between point charges q_i and q_j, in which the charge of O atom is $-2|e|$, and the charges of M atoms were $+2|e|$, $+2.67|e|$, $+3|e|$, $+4|e|$, $+5|e|$ and $+6|e|$ in MO, M_3O_4, M_2O_3, MO_2, M_2O_5 and MO_3, respectively. The latter terms were the standard Lennard-Jones and Born-Mayer terms. The parameters of A, B, C, and ρ were given in Table 1.

The curves of the different pair interactions of MO clusters are shown in Fig. 1. It is clear that in the figure the curve of coulomb contribution is similar to that of the pair potential. It means that the energy of MO clusters is mainly contributed by coulomb interaction. Therefore, it is necessary to investigate the influence of the charges of M atoms on the structures. The parameters of last three terms in Eq. (2) take the same values, and the values between aluminum and oxygen ions investigated previously are used for simplicity [21,23].

Table 1
Parameters of the potential energy function for metal (M) oxide (O) clusters.

Pair potential parameters	A(evÅ^{22})	ρ(Å)	B(eV)	C(evÅ^6)
M—M	1.0	/	0.000	0.000
M—O	10.0	0.2649	2409.505	0.000
O—O	1.0	0.1490	22764.000	27.88

2.2. Structural optimization of metal oxide clusters by the modified DLS method

The DLS method can be derived from the fact that only specific positions will be located after local minimization (LM) when one atom is added to a N-atom cluster. Therefore, on the surface of the N-atom cluster, the atom may occupy many lattice positions, and all possible lattice points are vacant DL. The DLS algorithm consists of three steps. The first step is to randomly generate one structure of a cluster, which will be further locally minimized by the limited-memory quasi-Newton method (L-BFGS). Then, the DL sites are constructed on the structure. Next, the DL searching operation is carried out to find the candidates with lower energy by moving the atoms with higher energy in the cluster to the DL sites with a lower energy. If a new structure with lower energy can be obtained, it will be taken as the starting structure, and the repetition of "DL construction" and "DL searching" is performed to find global minimal structures. Finally, the optimization will stop and the current best structure is taken as the result of this calculation.

In our previous DLS method, vacant DL sites are generated by performing LM on the sites of a large Mackay icosahedral shell covering the current cluster. In detail, a probe atom is put into each site, and the single atom is operated by LM, named as sub-LM, to determine the lattice position.

For the structural optimization of metal oxide clusters by DLS method, the modification is on the construction of vacant DL sites. Because there are two types of atoms, i.e., M- and O-type, the type of vacant DL sites should be considered. Near an M-type atom, the vacant DL site should be occupied by a O-type atom, and the corresponding ones around a O-type atom should be a M-type atom. For each atom, the Cartesian coordinates (x_i, y_i, z_i) of its probe atoms are calculated by the following equations [58]

$$\begin{aligned} z_i^{'} &= 1 - \frac{2i}{I} \\ x_i^{'} &= \sqrt{1 - z_i^{'2}}\cos\left(2\pi i\phi^{-1}\right) \\ y_i^{'} &= \sqrt{1 - z_i^{'2}}\sin\left(2\pi i\phi^{-1}\right) \end{aligned} \tag{3}$$

$$\begin{bmatrix} x_i \\ y_i \\ z_i \end{bmatrix} = r_{pl}\begin{bmatrix} x_i^{'} \\ y_i^{'} \\ z_i^{'} \end{bmatrix} + \begin{bmatrix} X \\ Y \\ Z \end{bmatrix} \tag{4}$$

where I is the number of the probe atoms for each atom in clusters, and i is an integer between 0 and I. The ϕ^{-1} defined as $(\sqrt{5}-1)/2$. The r_{pl} is a positive constant, and its value is less than the half of M—O bond length ($r_{pl} = 0.6$ in this work). The X, Y, Z are Cartesian coordinates of each atom in clusters. If the value of I is bigger, the ability to search the lattice location will be better. In fact, when $I = 3$, all lattice locations can be found in this work. Therefore, 3 N probe atoms are generated. The M- and O- type probe atoms are obtained by this way, and they are further optimized by sub-LM. The process of construction of vacant DL sites is plotted in Fig. 2a. Fig. 2b plots the structural variation of metal oxide clusters during the optimization by a run of the modified DLS method. The modified DLS method is used to determine the stable structures of metal oxide clusters.

3. Results and discussion

3.1. Efficiency of the method for metal oxide clusters

The efficiency of the modified DLS method for each metal oxide cluster was investigated, and the studied sizes of clusters ranged from 49 to 77. Fig. 3 shows the average number of local optimization required for obtaining the lowest energy of different metal oxide clusters within

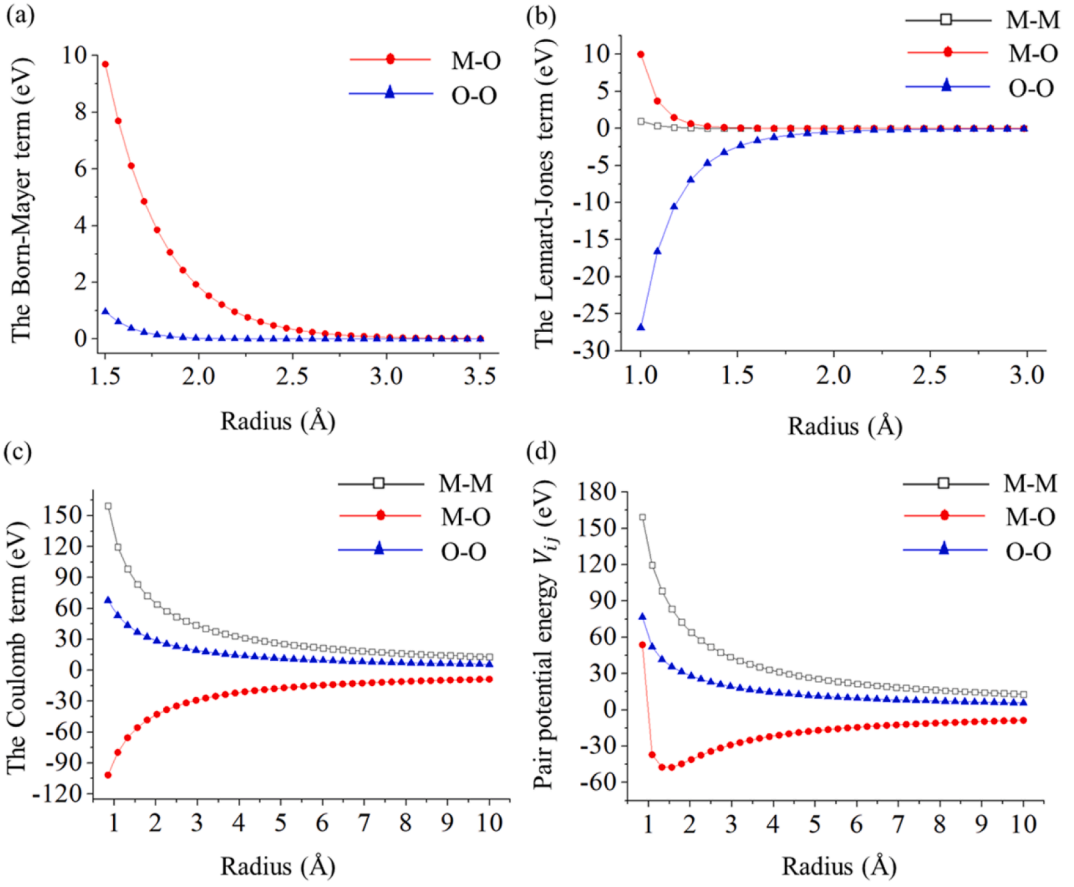

Fig. 1. The curves of the different pair interactions of metal (M) oxide (O) clusters. The Born-Mayer potential (a), the Lennard-Jones potential (b), the coulomb contribution (the formal charge of M is +3) (c), and pair potential energy V_{ij} (d).

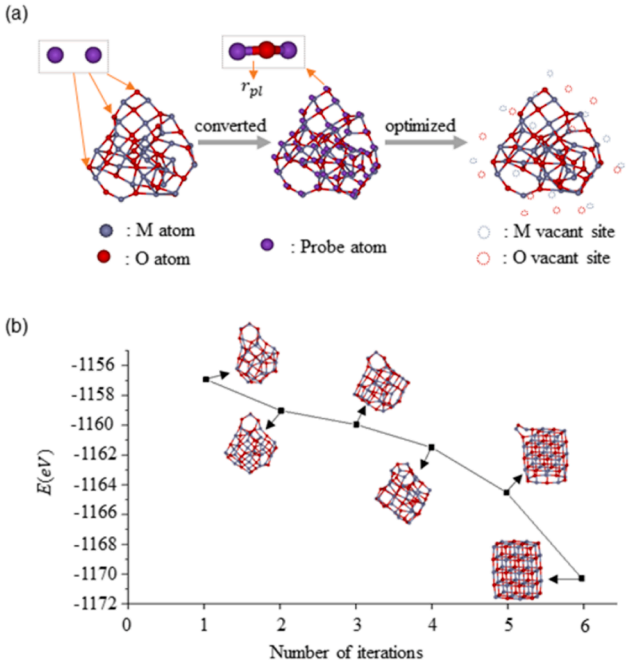

Fig. 2. Formation of vacant DL sites around the structure of a cluster (a), and the structural variation of metal oxide clusters during the optimization by a run of the modified DLS method (b).

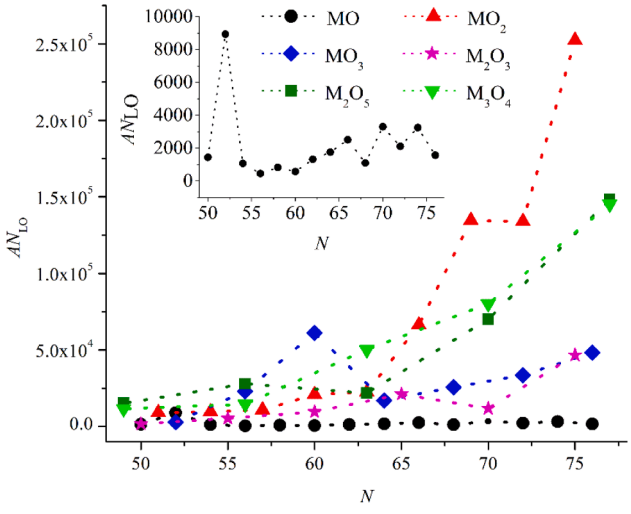

Fig. 3. The average number of local optimization (AN_{LO}) required for obtaining the global minimum of different metal oxide clusters with N atoms using the modified DLS method within 10,000 independent runs.

10,000 independent runs. In addition, the average number of local optimization and the hit number are provided in Supplementary material (see Table S1–S6). From Fig. 3 it can be seen that the average numbers of local optimization for MO clusters are significant lower than those for other metal oxides. This can be explained by the higher success rate for the structural optimization of MO clusters (see Table S1). Hence, the modified DLS method is suitable for locating the structures of MO

clusters with large sizes. However, for other metal oxide clusters, the efficiency of the algorithm is relatively low. Compared to other stochastic optimization algorithms, e.g., GA method [21], the modified DLS method still has advantages in convergence speed. It can be explained by the fact that DLS method takes the advantage of the modeling strategy and stochastic optimization [49]. In the DLS method, a simple greedy method (SGM) is utilized to optimize the surface atoms instead of the whole structure.

3.2. Structural optimization of metal oxide clusters

$(MO)_n$ clusters. The stable structures of $(MO)_n$ (n = 1–60) clusters with formal ionic charges of $M^{2+}O^{2-}$ are obtained by the modified DLS method and plotted in Fig. 4. Their point groups are also listed in the figure. From Fig. 4, it can be seen that these structures can be categorized into four classes, i.e., hexagonal tube, cage, cubic, composite structure of tube and cubic (e.g., n = 14). At n = 6, 9, 12, 15 and 21, clusters have hexagonal tube structures composed of six-member ring. The result is consistent with previous studies about $(MgO)_n$ clusters [9,10]. At n = 7, 8 and 11, clusters take cage structures. However, this cage structures disappear in large size $(MO)_n$ clusters. In Fig. 4, the dominant motif of $(MO)_n$ (n = 31–60) clusters is cubic. They can be approximately divided into three classes, i.e., prefect-cubic (e.g., n = 32), imperfect-cubic (e.g., n = 41), and composite structure of tube and cubic. In addition, it is clear that there is a trend from tube to perfect-cubic structures, and cubic structures are energetically preferable for large size clusters.

M_3O_4 clusters. The putative stable structures of $(M_3O_4)_n$ clusters (i.e., with the atomic ratio 3:4) are also optimized, in which the formal charge of metal set at + 2.67. Due to the limited search ability of the algorithm, the maximum size of optimization sets at n = 15. These stable structures of $(M_3O_4)_n$ (n = 1–15) clusters are shown in Fig. 5. It is clear that $(M_3O_4)_n$ clusters generally adopt cage-based structures. Compared to previous study on Fe_3O_4 clusters [59], there was significant difference

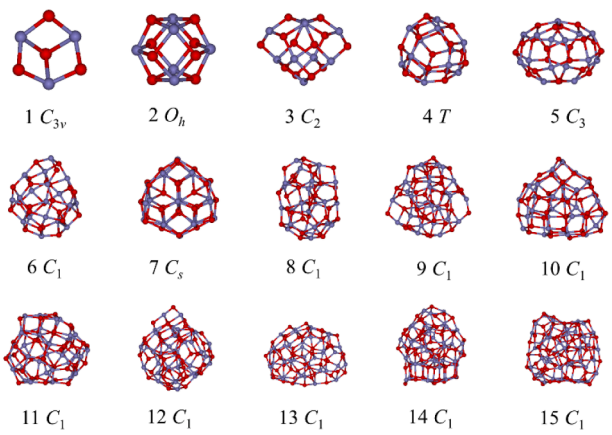

Fig. 5. Putative stable structures of $(M_3O_4)_n$ (n = 1–15) clusters.

between structures of $(M_3O_4)_n$ and $(Fe_3O_4)_n$ clusters. Within the smaller cluster sizes (n = 2–5), the Fe_3O_4 clusters took non-hollow structures, while hollow spherical cage for M_3O_4 clusters are favored in this study. Among the studied $(M_3O_4)_n$ clusters, two highly symmetrical structures are found, $(M_3O_4)_2$ with O_h symmetry and $(M_3O_4)_4$ cluster with T symmetry. When n reaches 6, the cage structures transform from hollow sphericity to non-hollow flat pattern. In addition, except for $(M_3O_4)_7$ with C_s symmetry, these clusters have C_1 symmetry.

M_2O_3 Clusters. The structures of $(M_2O_3)_n$ clusters (n = 1–20) have been optimized, and their stable structures were plotted in Fig. 6. Considering that $(M_2O_3)_n$ clusters adopt the parameters for $(Al_2O_3)_n$ clusters, the efficiency of the modified DLS algorithm can be verified by structural comparison. It was found that $(M_2O_3)_{1\text{-}15}$ and $(Al_2O_3)_{1\text{-}15}$ clusters had the same structures [21]. The $(M_2O_3)_1$, $(M_2O_3)_2$ and $(M_2O_3)_3$ clusters are kite-shaped, cage and tea-cozy motifs, respectively. The $(M_2O_3)_4$ structure is the superimposed by two surfaces, in which

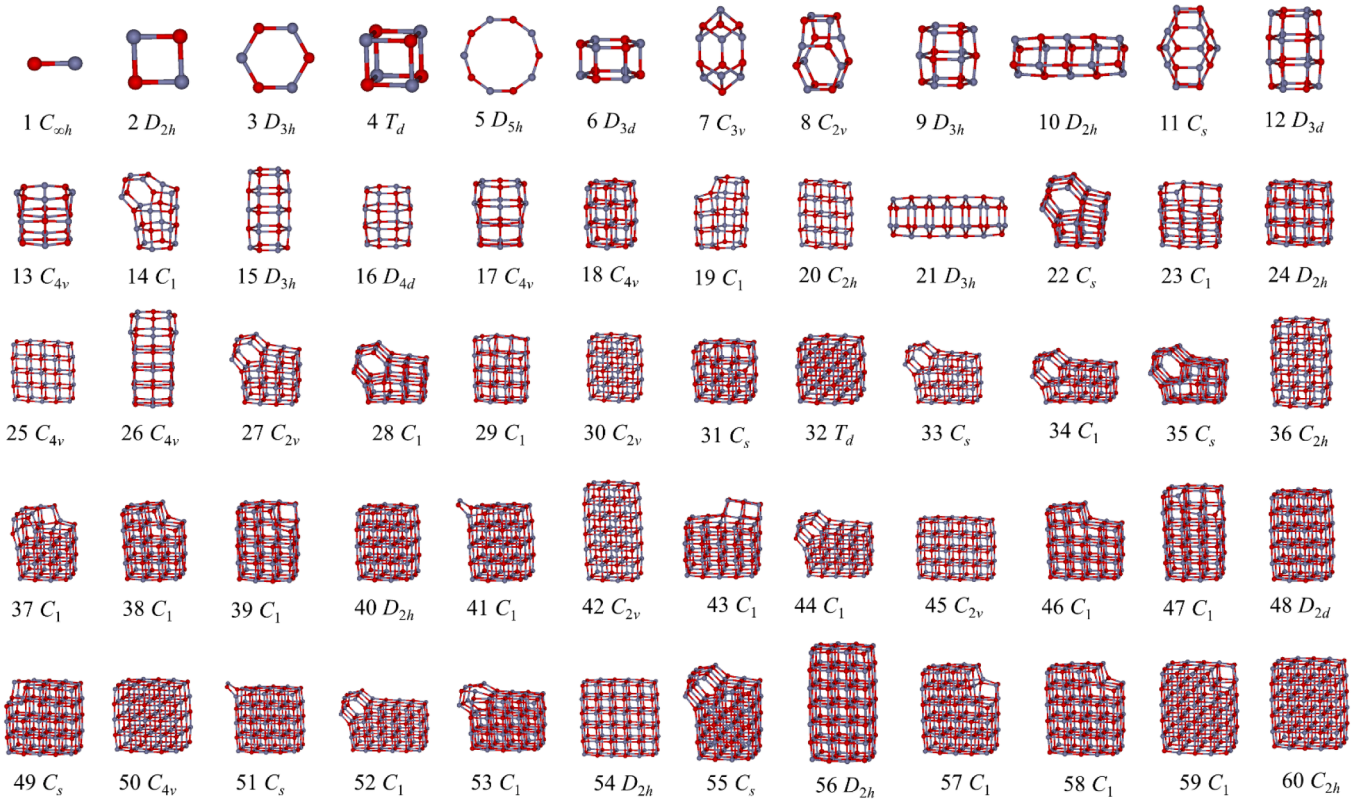

Fig. 4. Putative stable structures of $(MO)_n$ (n = 1–60) clusters, and O-atoms are represented by red spheres.

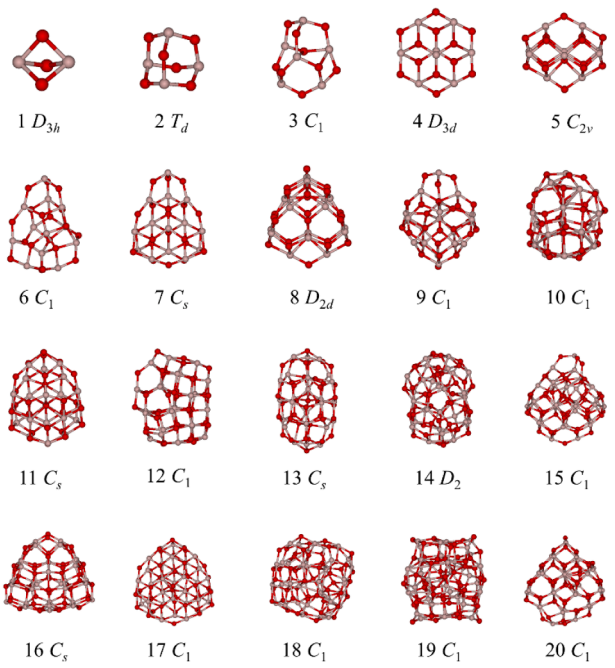

Fig. 6. Putative stable structures of $(M_2O_3)_n$ (n = 1–20) clusters.

each surface consists of three deformed-hexagons. For $(M_2O_3)_n$ (n = 6–7) clusters, the structures take tower layer motifs. A tetrahedral cage structure with D_{2h} point group is found for $(M_2O_3)_8$ cluster. For large size clusters i.e., n = 10–20, the structural fragments of small size clusters can be found. For instance, the $(M_2O_3)_{11}$ and $(M_2O_3)_{17}$ clusters are similar to $(M_2O_3)_7$ cluster, and the structures of $(M_2O_3)_{15}$ and $(M_2O_3)_{20}$ clusters are also similar to those of $(M_2O_3)_9$ and $(M_2O_3)_8$ clusters, respectively. In addition, the structure of $(M_2O_3)_{14}$ is found to be a heart-shaped one with D_2 symmetry. It can be seen that the structural types of the $(M_2O_3)_n$ clusters are more diverse than those of $(MO)_n$ and $(M_3O_4)_n$ clusters.

MO_2 Clusters. The stable structures of $(MO_2)_n$ (n = 1–40) clusters are further investigated as shown in Fig. 7. It can be seen that these studied structures include rhombus and deformed-triangle units, and they contain a large number of rhombic fragments. Especially, for small size clusters, i.e., n = 1–7, the lowest energy structures are incomplete closed motifs with one or two terminal O atoms (so-called dangling M═O bond) [15]. Interestingly, when n reaches 8, $(MO_2)_n$ cluster become closed structure, and the most stable structure of $(MO_2)_8$ is a hollow closed cage motif with C_{2h} symmetry. Furthermore, for larger clusters, i.e., n = 9–40, most of the clusters are disordered (or amorphous) structures. However, at $(MO_2)_{13}$ cluster, a highly symmetric structure with point group S_4 is found, and there are three tower layer motifs as lowest energy structures at n = 36–38. Among the three tower layer structures, although they have only C_1 symmetries, their structures have only one subunit, which is similar to $(M_2O_3)_2$ cluster.

M_2O_5 Clusters. The putative stable structures of $(M_2O_5)_n$ (n = 1–15) clusters are plotted in Fig. 8. From the figure, it is clear that M═O bonds are often found in these structures. Unlike $(MO_2)_n$ clusters, with increasing sizes, the M═O units do not disappear, but their number increases to 3 or 4. For $(M_2O_5)_2$ cluster, the structure takes cage motif (T_d symmetry) with four M═O bonds on the four sides, which is similar to $(M_2O_3)_2$ cluster. It is interesting to note that the clusters with n = 3–5 still take this motif that is similar to $(M_2O_3)_2$ as the structural unit, in which the number of the unit is two, three and four, and the number of the dangling bond is four, three and four, respectively. Starting from n = 7, the lowest energy structures are disordered. It is possible that the program does not fully explore the potential surface of $(M_2O_5)_n$ clusters.

MO_3 Clusters. The stable structures of the investigated $(MO_3)_n$ (n = 1–30) clusters are shown in Fig. 9. For the small size clusters, i.e., n = 1–5, the lowest energy structures have three or four M = O bonds. A highly symmetric structure with point group O_h is found at $(MO_3)_6$, which is a hollow spheroidal cage structure with six M = O bonds.

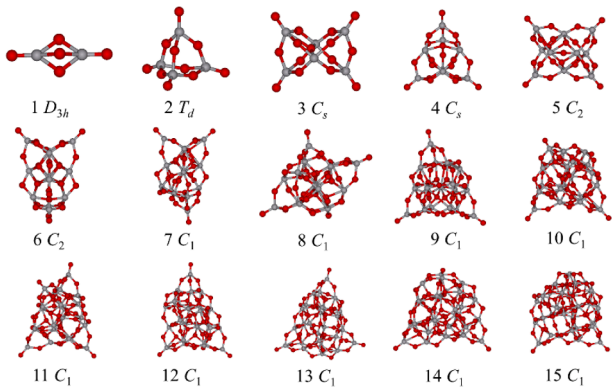

Fig. 8. Putative stable structures of $(M_2O_5)_n$ (n = 1–15) clusters.

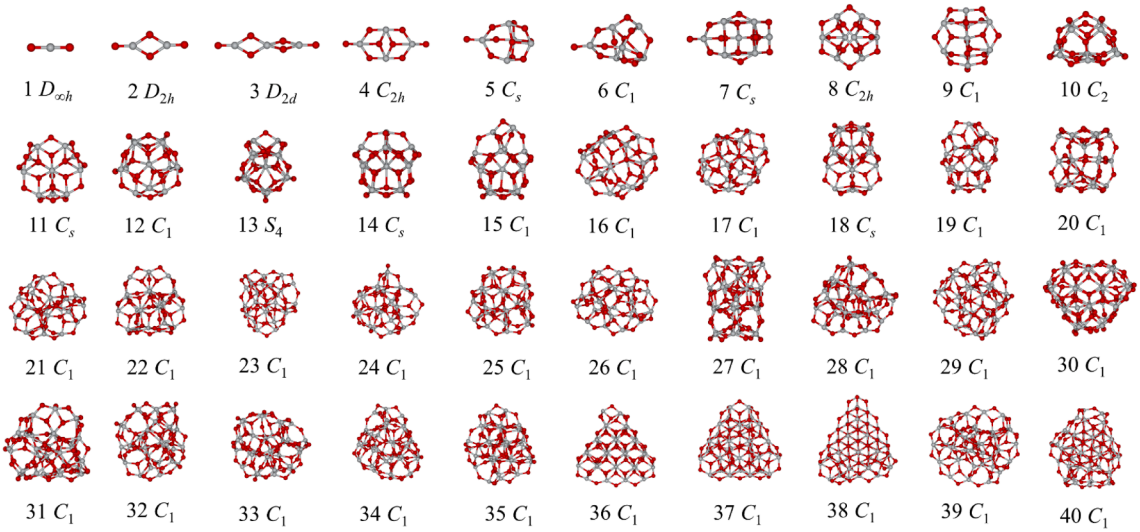

Fig. 7. Putative stable structures of $(MO_2)_n$ (n = 1–40) clusters.

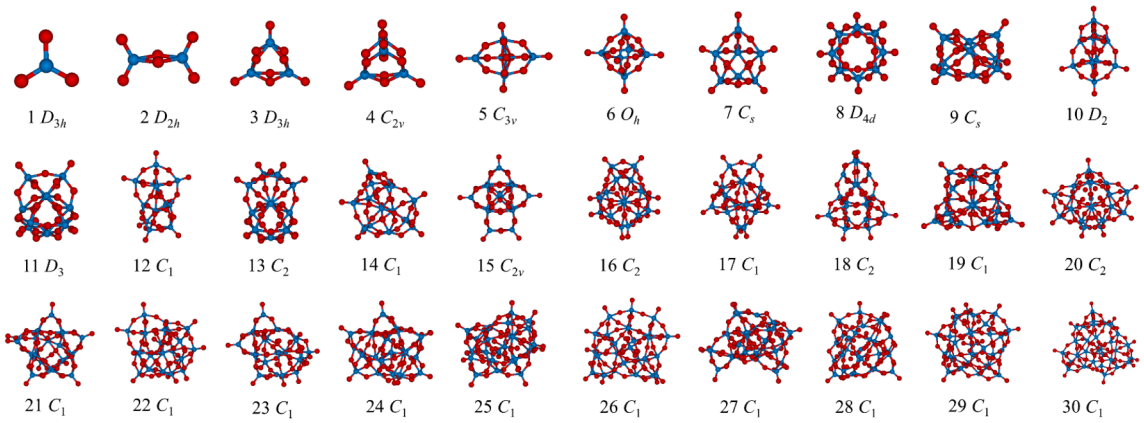

Fig. 9. Putative stable structures of $(MO_3)_n$ (n = 1–30) clusters.

Except for $(MO_3)_8$ cluster, the number of M═O bonds is also six for the clusters with n = 7–11. The most stable structure of $(MO_3)_8$ cluster takes hollow cage with D_{4h} symmetry, having eight M═O bonds. The structures owning eight M═O bonds are also found at n = 12–16 and18. When n = 19, the number of M═O bond is more than eight. It was found that compared with $(M_2O_5)_n$ clusters, the $(MO_3)_n$ clusters have more dangling bonds, and the number of the bonds increases with the increasing size n. In addition, the bond length of M═O in $(MO_3)_n$ clusters is approximately 1.2 Å, and it is shorter than those of previous studies on MO_3 clusters (e.g., the corresponding values for Cr, Mo and W are approximately 1.55 Å, 1.69 Å, and 1.71 Å, respectively). Considering that the parameters of the model potential are used here, the difference of bond lengths between the model potential and the real systems is reasonable.

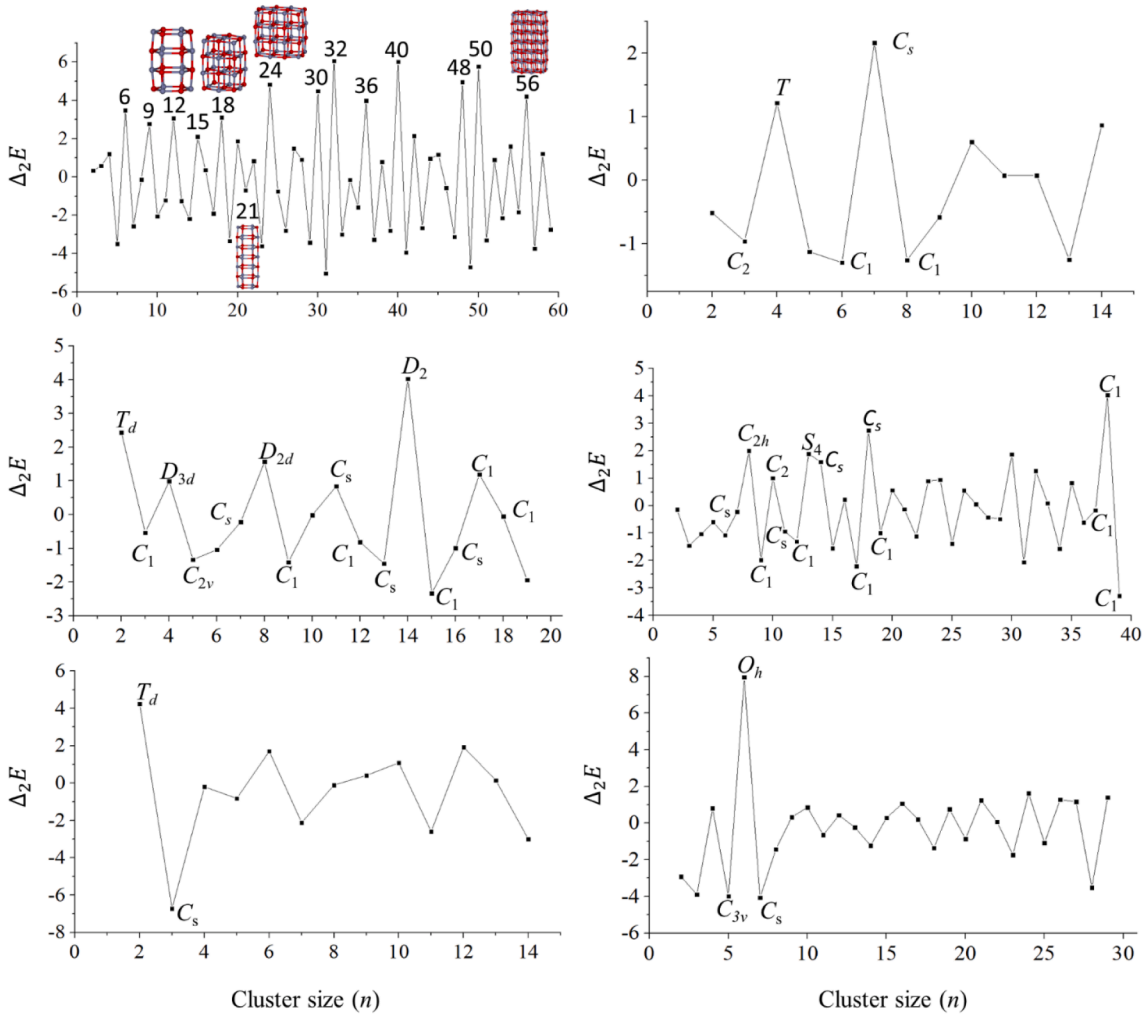

Fig. 10. The second finite difference (Δ_2E) of the energy of $(MO)_n$ (a), $(M_3O_4)_n$ (b), $(M_2O_3)_n$ (c), $(MO_2)_n$ (d), $(M_2O_5)_n$ (e) and $(MO_3)_n$ (f) clusters.

3.3. Relative stability of metal oxide clusters

To investigate the stability of metal oxide clusters comparing to their neighbors, the second finite difference (Δ_2E) of the energy is applied as a quantitative function, and defined as follow:

$$\Delta_2E(n) = E(n+1) + E(n-1) - 2E(n) \quad (5)$$

where $E(n+1)$, $E(n-1)$ and $E(n)$ are the potential energies of $n+1$, n-1 and n– atom metal oxide clusters, respectively. Fig. 10 plots the Δ_2E values for $(MO)_n$ (n = 1–60), $(M_3O_4)_n$ (n = 1–15), $(M_2O_3)_n$ (n = 1–20), $(MO_2)_n$ (n = 1–40), $(M_2O_5)_n$ (n = 1–15) and $(MO_3)_n$ (n = 1–30) clusters. In the figure, some positive peaks appear on specific cluster sizes, which correspond to particularly stable structures with respect to their neighbors. From the curve of $(MO)_n$ clusters (Fig. 10a), the positive peaks are found at n = 6, 9, 12, 15 18, 24, 30 and 56). It can be clearly found that the stacked hexagonal rings occupy those peaks at smaller clusters, i.e., n = 1–17, while the larger size clusters tend to take cuboidal structures. At $(MO)_{21}$ cluster, although the structure is also stacked hexagonal ring, the Δ_2E is negative, indicating that the structure is unstable with respect to its neighbors. The results are in agreement with previous studies about $(MgO)_n$ clusters [10]. For large clusters, i.e., n = 30–60, the perfect-cuboids are relatively more stable. However, this conclusion is not applicable to all $(MO)_n$ clusters. For instance, in the studied $(ZnO)_n$ clusters by Woodley [35], cage motifs were almost found though their clusters with hexagonal rings also tended to have lower energies as in this study.

On the other hand, $(MO)_n$ clusters with higher symmetry tend to be relatively more stable as seen in Fig. 10. From the Fig. 10c, eight positive peaks, i.e., n = 2, 4, 8, 11, 14, and 17, are found in $(M_2O_3)_n$ clusters. These clusters have higher point group symmetry, e.g., T_d for $(M_2O_3)_2$, D_{3d} for $(M_2O_3)_4$, D_{2d} for $(M_2O_3)_8$, and D_2 for $(M_2O_3)_{14}$. In addition, T for $(M_3O_4)_4$ in $(M_3O_4)_n$, S_4 for $(MO_2)_{13}$ in $(MO_2)_n$ clusters, T_d for $(M_2O_5)_2$ in $(M_2O_5)_n$ clusters, and O_h for $(MO_3)_6$ in $(MO_3)_n$ clusters are also found. Exceptionally, the $(MO)_{21}$ cluster with D_{3h} symmetry is less stable than $(MO)_{22}$ cluster with C_S symmetry. Though $(M_2O_3)_{17}$ cluster is only C_1 symmetry, it is more stable than $(M_2O_3)_{16}$ cluster with C_s symmetry.

3.4. Geometrical evolution of metal oxide clusters with the formal charge of metal

The investigated metal oxide clusters are divided into two types according to the formal charge of metal, that is, lower and higher q value clusters. The lower q value clusters include $(MO)_n$, $(M_3O_4)_n$, and $(M_2O_3)_n$, and the remaining structures are considered higher q value clusters. Fig. 11 plots the variation of the structural motifs with respect to q value. The lower q value clusters correspond to three straight lines with zero ordinates in the figure, which means that no M═O fragments in structures. However, when the q value reaches + 4, the structures with M═O fragments emerge at small size, while M═O fragments disappear at larger clusters. When q = +5, all $(M_2O_5)_n$ clusters own M═O fragments, and the numbers are two, three or four. When the q value reaches +6, the number of M═O fragments of $(MO_3)_1$ clusters is three, and there exists an upward trend on the whole with the increasing value of n in $(MO_3)_n$ clusters. Therefore, in metal oxide clusters with larger q values, M═O fragments are often found.

4. Conclusion

In this paper, a modified dynamic lattice searching (DLS) method was developed to study the stable structures of metal oxide clusters. To adapt to coexistence of M- and O-type atoms, a new method of constructing dynamic lattice sites was proposed. The classical empirical potential was applied to explore the effects of q value (i.e., formal charge of metal) on the structures of metal oxide clusters systematically. The investigated metal oxide clusters included $(M^{+2}O)_n$ (n = 1–60),

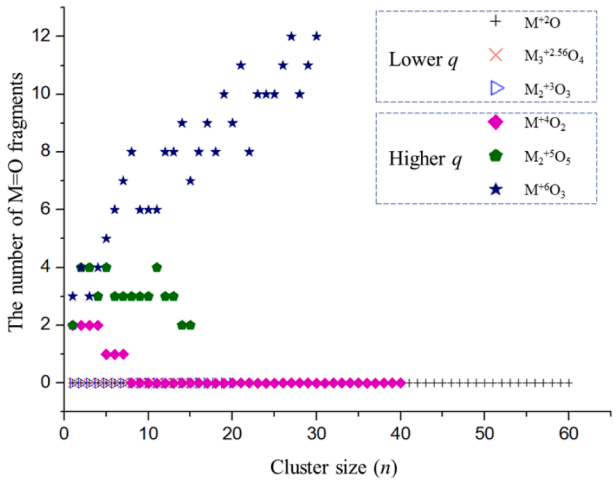

Fig. 11. Schematic diagram of the evolution of metal oxide clusters with respect to q values.

$(M_3^{+2.67}O_4)_n$ (n = 1–15), $(M_2^{+3}O_3)_n$ (n = 1–20), $(M^{+4}O_2)_n$ (n = 1–40), $(M_2^{+5}O_5)_n$ (n = 1–15) and $(M^{+6}O_3)_n$ (n = 1–30) clusters. The growth rules of MO clusters for different q values were studied, and the differences of structures and relative stability were discussed. Results showed that the $(MO)_n$ clusters are favorable to form highly coordinated structures. For higher q value clusters, e.g., $(M_2O_5)_n$ and $(MO_3)_n$ clusters, the structures tend to carry multiple M═O fragments, and the number of M═O fragments increases with the increasing q values.

Declaration of Competing Interest

The authors declare that they have no known competing financial interests or personal relationships that could have appeared to influence the work reported in this paper.

Acknowledgments

This study is supported by National Natural Science Foundation of China (NSFC) (Grant Nos. 21873001), Key University Science Research Project of Anhui Province (Grand No. KJ2017A349), and by the Foundation of Distinguished Young Scientists of Anhui Province. The calculations are carried out at the High-Performance Computing Center of Anhui University.

Appendix A. Supplementary data

Supplementary data to this article can be found online at https://doi.org/10.1016/j.chemphys.2021.111097.

References

[1] R.S. Devan, R.A. Patil, J.H. Lin, Y.R. Ma, Adv. Funct. Mater. 22 (2012) 3326.
[2] Ü. Özgür, Y.I. Alivov, C. Liu, A. Teke, M. Reshchikov, S. Doğan, V. Avrutin, S. J. Cho, H. Morkoç, J. Appl. Phys. 98 (2005) 11.
[3] C. Sun, L.-M. Liu, A. Selloni, G.Q.M. Lu, S.C. Smith, J. Mater. Chem. 20 (2010) 10319.
[4] D.R. Miller, S.A. Akbar, P.A. Morris, Sens. Actuators, B 204 (2014) 250.
[5] E. Comini, C. Baratto, I. Concina, G. Faglia, M. Falasconi, M. Ferroni, V. Galstyan, E. Gobbi, A. Ponzoni, A. Vomiero, Sens. Actuators, B 179 (2013) 3.
[6] X. Fuku, K. Kaviyarasu, N. Matinise, M. Maaza, Nanoscale Res. Lett. 11 (2016) 1.
[7] B. Wang, S. Nagase, J. Zhao, G. Wang, J. Phys. Chem. C 111 (2007) 4956.
[8] S. Zhang, Y. Zhang, S. Huang, H. Liu, P. Wang, H. Tian, J. Mater. Chem. 21 (2011) 16905.
[9] M. Haertelt, A. Fielicke, G. Meijer, K. Kwapien, M. Sierka, J. Sauer, Phys. Chem. Chem. Phys. 14 (2012) 2849.
[10] R. Dong, X. Chen, X. Wang, W. Lu, J. Chem. Phys. 129 (2008), 044705.
[11] S.F. Vyboishchikov, J. Sauer, J. Phys. Chem. A 105 (2001) 8588.
[12] S. Feyel, J. Döbler, D. Schröder, J. Sauer, H. Schwarz, Angew. Chem. Int. Ed. 45 (2006) 4681.

[13] M. Calatayud, L. Maldonado, C. Minot, J. Phys. Chem. C 112 (2008) 16087.
[14] S. Woodley, S. Hamad, J. Mejias, C. Catlow, J. Mater. Chem. 16 (2006) 1927.
[15] S. Hamad, C. Catlow, S. Woodley, S. Lago, J. Mejias, J. Phys. Chem. B 109 (2005) 15741.
[16] A.B. Hernández, W.I. Hernández, A.P. Cid, J.C. García, M.S. Villanueva, Comput. Mater. Sci. 162 (2019) 228.
[17] X. Tang, D. Bumueller, A. Lim, J. Schneider, U. Heiz, G. Ganteför, D.H. Fairbrother, K.H. Bowen, J. Phys. Chem. C 118 (2014) 29278.
[18] L. Sai, L. Tang, X. Huang, G. Chen, J. Zhao, J. Wang, Chem. Phys. Lett. 544 (2012) 7.
[19] A.B. Rahane, M.D. Deshpande, J. Phys. Chem. C 116 (2012) 2691.
[20] X.-L. Ding, W. Xue, Y.-P. Ma, Z.-C. Wang, S.-G. He, J. Chem. Phys. 130 (2009), 014303.
[21] Q. Zhang, L. Cheng, J. Chem. Inf. Model 55 (2015) 1012.
[22] L. Ren, L. Cheng, Y. Feng, X. Wang, J. Chem. Phys. 137 (2012), 014309.
[23] S.M. Woodley, Proc. R. Soc. A 467 (2011) 2020.
[24] Y. Yuan, L. Cheng, Int. J. Quantum Chem. 113 (2013) 1264.
[25] A.B. Rahane, P.A. Murkute, M.D. Deshpande, V. Kumar, J. Phys. Chem. A 117 (2013) 5542.
[26] X.-L. Ding, Z.-Y. Li, J.-H. Meng, Y.-X. Zhao, S.-G. He, J. Chem. Phys. 137 (2012), 214311.
[27] H. Yuan, H. Chen, C. Tian, A. Kuang, J. Wang, J. Chem. Phys. 140 (2014), 154308.
[28] S. Hosseini, M. Vahedpour, M. Shaterian, M.A. Rezvani, Phys. Chem. Res. 6 (2018) 493.
[29] X. Xia, W. Hu, Y. Shao, J. Phys. Chem. C 119 (2015) 8349.
[30] H.-J. Zhai, S. Li, D.A. Dixon, L.-S. Wang, J. Am. Chem. Soc. 130 (2008) 5167.
[31] S. Li, J.M. Hennigan, D.A. Dixon, K.A. Peterson, J. Phys. Chem. A 113 (2009) 7861.
[32] C. Roberts, R.L. Johnston, Phys. Chem. Chem. Phys. 3 (2001) 5024.
[33] R.B. Wang, S. Körbel, S. Saha, S. Botti, N.V. Skorodumova, J. Phys. Chem. C 121 (2017) 9528.
[34] R. Li, L. Cheng, Comput. Theor. Chem. 996 (2012) 125.
[35] A.A. Al-Sunaidi, A.A. Sokol, C.R.A. Catlow, S.M. Woodley, J. Phys. Chem. C 112 (2008) 18860.
[36] L. Zibordi-Besse, Y. Seminovski, I. Rosalino, D. Guedes-Sobrinho, J.L. Da Silva, J. Phys. Chem. C 122 (2018) 27702.
[37] D.J. Wales, J.P. Doye, J. Phys. Chem. A 101 (1997) 5111.
[38] C. Loschen, A. Migani, S.T. Bromley, F. Illas, K.M. Neyman, Phys. Chem. Chem. Phys. 10 (2008) 5730.
[39] Y. Zhao, X. Chen, J. Li, Nano Res. 10 (2017) 3407.
[40] C. Kerpal, D.J. Harding, A.C. Hermes, G. Meijer, S.R. Mackenzie, A. Fielicke, J. Phys. Chem. A 117 (2013) 1233.
[41] H.-J. Zhai, J. Döbler, J. Sauer, L.-S. Wang, J. Am. Chem. Soc. 129 (2007) 13270.
[42] J. Carrasco, F. Illas, S.T. Bromley, Phys. Rev. Lett. 99 (2007), 235502.
[43] N. Marom, M. Kim, J.R. Chelikowsky, Phys. Rev. Lett. 108 (2012), 106801.
[44] G. Santambrogio, E. Janssens, S. Li, T. Siebert, G. Meijer, K.R. Asmis, J. Döbler, M. Sierka, J. Sauer, J. Am. Chem. Soc. 130 (2008) 15143.
[45] J. Zhang, M. Dolg, Phys. Chem. Chem. Phys. 17 (2015) 24173.
[46] M. Ju, J. Lv, X.-Y. Kuang, L.-P. Ding, C. Lu, J.-J. Wang, Y.-Y. Jin, G. Maroulis, RSC Adv. 5 (2015) 6560.
[47] X. Wu, W. Cai, X. Shao, Chem. Phys. 363 (2009) 72.
[48] X. Yang, W. Cai, X. Shao, J. Comput. Chem. 28 (2007) 1427.
[49] X. Shao, L. Cheng, W. Cai, J. Comput. Chem. 25 (2004) 1693.
[50] L. Cheng, J. Yang, J. Phys. Chem. A 111 (2007) 5287.
[51] X. Shao, X. Wu, W. Cai, J. Phys. Chem. A 114 (2010) 12813.
[52] X. Shao, X. Wu, W. Cai, J. Phys. Chem. A 114 (2010) 29.
[53] X. Wu, C. He, Chem. Phys. 405 (2012) 100.
[54] L. Cheng, W. Cai, X. Shao, Chem. Phys. Chem. 6 (2005) 261.
[55] X. Wu, W. Cheng, J. Chem. Phys. 141 (2014), 124110.
[56] X. Wu, Y. Dong, New J. Chem. 38 (2014) 4893.
[57] K. Yu, X. Wang, L. Chen, L. Wang, J. Chem. Phys. 151 (2019), 214105.
[58] R. Marques, C. Bouville, M. Ribardière, L.P. Santos, K. Bouatouch, Comput. Graphics Forum (2013) 134.
[59] R. Mejia-Olvera, J. Reveles, S. Pacheco-Ortín, J. Santoyo-Salazar, Chem. Phys. Lett. 706 (2018) 494.